# Coherent optical association of a single molecule

Yichao Yu,[1, 2, 3, *] Kenneth Wang,[1, 2, 3] Jonathan D. Hood,[4] Lewis R. B. Picard,[1, 2, 3] Jessie T. Zhang,[1, 2, 3] William B. Cairncross,[2, 1, 3] Jeremy M. Hutson,[5] Till Rosenband,[1] and Kang-Kuen Ni[2, 1, 3, †]

[1]*Department of Physics, Harvard University, Cambridge, Massachusetts 02138, USA*
[2]*Department of Chemistry and Chemical Biology, Harvard University, Cambridge, Massachusetts 02138, USA*
[3]*Harvard-MIT Center for Ultracold Atoms, Cambridge, Massachusetts 02138, USA*
[4]*Department of Chemistry, Purdue University, West Lafayette, Indianna, 47906*
[5]*Joint Quantum Centre Durham-Newcastle, Department of Chemistry,*
*Durham University, Durham, DH1 3LE, United Kingdom*
(Dated: October 29, 2020)

We report on coherent association of a single weakly-bound NaCs molecule in an optical tweezer through an optical Raman transition without the use of a Feshbach resonance. The Raman scheme uses a deeply bound electronic excited intermediate state to achieve a large transition dipole moment while reducing the photon scattering. Starting from two atoms in their relative motional ground state, we achieve an optical transfer efficiency of 69%. The molecule has a binding energy of 770.200516(24)MHz at 8.8 G (Unresolved comment from Jon: with so many digits on the resonance frequency, we may need to mention more digits on the B field number and/or also state the tweezer power. We can state the tweezer power for where we measure it, but the transmission through the objective, etc. I believe is only estimated.) with more than 60% of the molecule created in the motional ground state. This technique does not rely on narrow excited state lines or Feshbach resonances and will allow a wider range of molecular species to be assembled atom-by-atom.

Diverse species of fully quantum controlled ultracold molecules are desired for a wide variety of applications including precision measurements [1–6], quantum simulations [7–10], quantum information processing [11–14], and studies of ultracold chemistry [15–18]. While many innovative approaches demonstrated in the last few years have directly cooled different species of diatomic or polyatomic molecules below 1 mK [19–24], the coldest and the highest phase-space-density gas to date in an ensemble [25] or as individuals [26, 27] have been achieved through the association of ultracold atoms.

Molecular association of ultracold atoms takes advantage of the cooling and trapping techniques that have been developed for atoms. Associating atoms into deeply-bound molecules is challenging because of the small wavefunction overlap between the free-atom and molecular state and the release of a large amount of binding energy. A two-step approach has been demonstrated to first associate atom pairs into weakly-bound molecules, and then transfer the molecules from this single internal state to a desired rovibrational and electronic state releasing the binding energy via stimulated emission [1, 28–35]. So far, most molecular association has been achieved for bialkali molecules by magnetoassociation using a magnetic Feshbach scattering resonance. The only exceptions are $Sr_2$, where narrow linewidth ($\sim 20$ kHz) excited states are available and optical association can be driven coherently, [36, 37] and $^{87}Rb^{85}Rb$, where weakly bound molecules with a couple MHz binding energy exists [27]. With these requirements, dimers between alkali atoms and non-magnetic atoms, or molecules involving atoms without narrow intercombination lines remain difficult to associate.

Here, we demonstrate coherent association of an atom pair to a weakly bound molecule using a two-photon optical Raman transfer via an electronic excited state, schematically shown in Fig. 1A. The scheme does not rely on a Feshbach resonance, few MHz level bound states, or a narrow excited state. The resulting single molecule is in a well-defined internal quantum state and predominately in its motional ground state. A vibrational state of the electronic excited state $c^3\Sigma^+(\Omega = 1)$ is used as the intermediate state in the Raman scheme, and is chosen to minimize the theoretical photon scattering during a Raman Rabi oscillation. To further reduce the photon scattering and sensitivity to laser intensity noise, we choose the initial and final state to balance the two Rabi frequencies as much as possible. This system-independent approach can be used for creating new molecules atom-by-atom with full quantum state control.

The essence of an optical Raman transfer can be illustrated using a three-level system (Fig. 1A), where the initial atomic state, and the target weakly-bound molecular state are coupled to an intermediate state by two laser frequencies with Rabi frequencies, $\Omega_a$ and $\Omega_m$, with one-photon detuning $\Delta$, and two-photon detuning, $\delta$. The transfer Raman Rabi Rate, $\Omega_R = \Omega_a\Omega_m/2\Delta$, is accompanied by a photon scattering rate $\Gamma_s$ [38]. Unlike Raman transitions in atoms, the two Rabi frequencies are greatly imbalanced due to the small wavefunction overlap between the atomic state and the intermediate state, and therefore the scattering is predominantly from the target molecular state. Furthermore, the energy difference between the atomic state and target molecular state is small ($< 1$ GHz) compared to the single photon detuning, $\Delta$, so the target molecular state can scatter off both
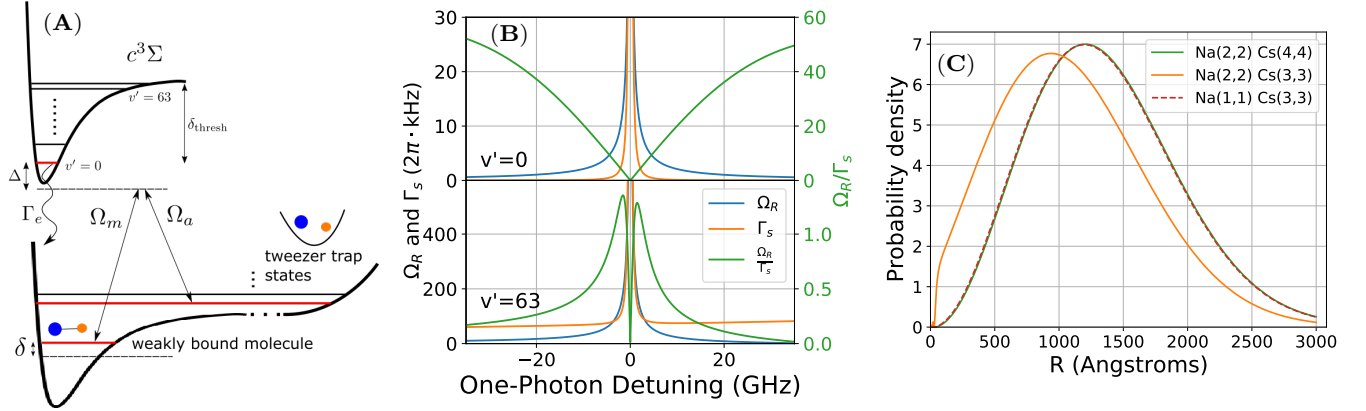
FIG. 1. Optical creation of single molecule from single atoms in tweezer. (A) Schematics of the optical transition from an atom pair to a weakly bound molecule. The initial state is the relative motional ground state between the two atoms and the final state is the first molecular bound state. The transition is driven by a pair of laser frequencies matching the binding energy of the molecule. The lasers are detuned from an excited molecular state in the $c^3\Sigma$ potential by $\Delta$ in order to suppress the scattering during the transfer. (B) Comparison between using a weakly bound and a deeply bound excited state as intermediate state for the Raman transition. The deeply bound excited state (upper half $v' = 0$) has a smaller Raman Rabi frequency ($\Omega_R$) compared to the weakly bound excited state (lower half $v' = 63$) at a given detuning. However, the scattering rate ($\Gamma_s$) is also much lower, which results in a larger Raman Rabi frequency to scattering rate ratio. (C) Enhancement of short range wavefunction. The large scattering length for the $Na(2,2), Cs(3,3)$ state creates an interaction shift comparable to the axial trapping frequency. This causes a significant change in the relative wavefunction especially at short intranuclear distance ($R$). Compared to other spin states with weaker interaction, the wavefunction at short distance ($R < 100$Å) is significantly enhanced.

beams roughly equally. Thus, the scattering is given by $\Gamma_s = \Gamma_e \Omega_m^2/2\Delta^2$, where $\Gamma_e$ is the excited state linewidth [39]. The ratio between the Raman Rabi frequency and the scattering rate is therefore $\Omega_a/\Omega_m \times \Delta/\Gamma_e$. To ensure a coherent process, a detuning as large as possible, while maintaining a realistic Raman Rabi frequency, is preferred.

Early experiments used weakly-bound excited states as the intermediate state in the Raman transition to ensure a large Raman Rabi frequency [40, 41]. However, for a complete picture, the many excited vibrational states in a molecular potential as well as the excited atomic continuum need to be considered. The total scattering rate and Raman Rabi rate become a sum of the scattering rates and Raman Rabi rates over all possible intermediate states. With these considerations, using a weakly-bound excited state as the intermeidate state suffers from strong scattering of the nearby excited atomic continuum rendering it incoherent, resulting in molecule loss. This scattering is proportional to $1/\delta_{thresh}^2$, where $\delta_{thresh}$ is the detuning from the dissociation threshold, and thus can be made smaller by detuning away from the dissociation threshold.

To find the optimal intermediate state, we perform a calculation of the Raman Rabi frequency and scattering rate at different detunings from the atomic threshold taking into account of all states of the $c^3\Sigma^+(\Omega = 1)$ excited molecular state potential [42] and the continuum [43]. The excited atomic continuum is particularly important for the target molecular state. The sum of the

squares of the wavefunction overlap between the target weakly-bound molecular state and all the excited molecular intermediate states considered is only about 2%, suggesting that there is significant matrix element between the target molecular state and the excited atomic continuum (See SM). This calculation shows that the ratio of the Raman Rabi rate to scattering rate can be made larger for more deeply bound states compared to weakly bound states at a cost of a smaller Raman Rabi frequency (Fig. 1B, full result in SM) As a result, we choose the $v' = 0$ of $c^3\Sigma^+(\Omega = 1)$ as an intermediate state to drive the Raman transition.

In addition to the intermediate state, choosing an initial and a final state for a large $\Omega_a/\Omega_m$ ratio would allow large Raman Rabi coupling at a given detuning. Furthermore, a larger ratio also relaxes the intensity stability requirement, because this is also the ratio between the Raman Rabi coupling and the AC Stark shift of the molecular state, $\Omega_m^2/2\Delta$ [44]. Due to the small size of the intermediate state wavefunction, the coupling $\Omega_a$ is approximately proportional to the value of the relative atomic wavefunction at short distance within the molecular potential. To increase the amplitude within the molecular potential, one can increase the external confinement of atom pairs. Using a harmonic oscillator approximation, the short range amplitude is proportional to $\omega_{trap}^{3/4}$, where $\omega_{trap}$ is the trap frequency. Alternatively, one can choose an atomic pair state with a large scattering length (positive or negative). For these states, the phase shift in the relative wavefunc-

tion between the atoms can significantly increase the short range wavefunction (Fig. 1C). For our system of Na and Cs atoms, we choose a spin state combination $|\uparrow_{Na}\downarrow_{Cs}\rangle \equiv |F = 2, m_F = 2\rangle_{Na} |F = 3, m_F = 3\rangle_{Cs}$ that has a large and negative scattering length of $a(\uparrow_{Na}\downarrow_{Cs}) = -693.8a_0$ [45]. We note that other stable spin combinations give smaller scattering lengths ($< 50\, a_0$). In addition to the increased atomic coupling, $\Omega_a$, coupled channel calculations show that the target molecular state that is predominantly in this spin combination also has reduced coupling, $\Omega_m$, with the intermediate state when compared to bound states of the other stable spin combinations Therefore, using an initial $|\uparrow_{Na}\downarrow_{Cs}\rangle$ hyperfine combination results in a $\Omega_a/\Omega_m$ ratio of about 0.05 instead of a ratio of about 0.003 with the other combinations, and thus only an required intensity stability of 5% instead of 0.3%. (clean up the paragraph some more).

Experimentally, we first prepare two atoms in a well-defined external and internal quantum state using techniques developed previously [46–48]. In brief, the experimental cycle begins by stochastically loading a single $^{23}$Na atom and a single $^{133}$Cs atom into separate optical tweezers. The atoms are initially imaged to distinguish between loading of two atoms, one atom (Na or Cs), or no atom to be able to post select the experimental result on the initial loading condition. Raman sideband cooling is then applied to cool both atoms simultaneously into the 3-dimensional motional ground state of their optical tweezers. After cooling, the Na and Cs atoms are in a spin state of $|\uparrow_{Na}\uparrow_{Cs}\rangle \equiv |F = 2, m_F = 2\rangle_{Na} |F = 4, m_F = 4\rangle_{Cs}$ which has a low scattering length. The small two atom interaction allows the two atoms to be merged into the same tweezer with minimum pertubation and remain in the motional ground state after the merge.

Next, we drive the atoms into the large scattering length $|\uparrow_{Na}\downarrow_{Cs}\rangle$ hyperfine combination to use as the initial atomic state of Raman transfer by performing a Cs spin flip while taking into account the $-30.7kHz$ interaction shift [45]. This spin flip selectively transfers atoms in the relative motion ground state [49], and for the experiment reported here, this is 31% of the initial population of two atoms loaded in separate optical tweezers.

To perform Raman transfer of an atom pair to the target weakly-bound molecular state, we use the tweezer itself as the Raman beams by turning on two co-propagating frequencies in the tweezer during the Raman pulse (Fig. 2A). The dual use of the tweezer beam not only eliminates additional scattering sources or undesired laser frequencies, but also allows a tight focus to maximize the Raman Rabi frequency and minimize the transfer time. The pulse sequence is shown in Fig. 2B. After the total tweezer power is set to the desired value, we smoothly ramp down the power of one frequency in the tweezer while simultaneously ramping up the power of a different frequency so that the total tweezer power
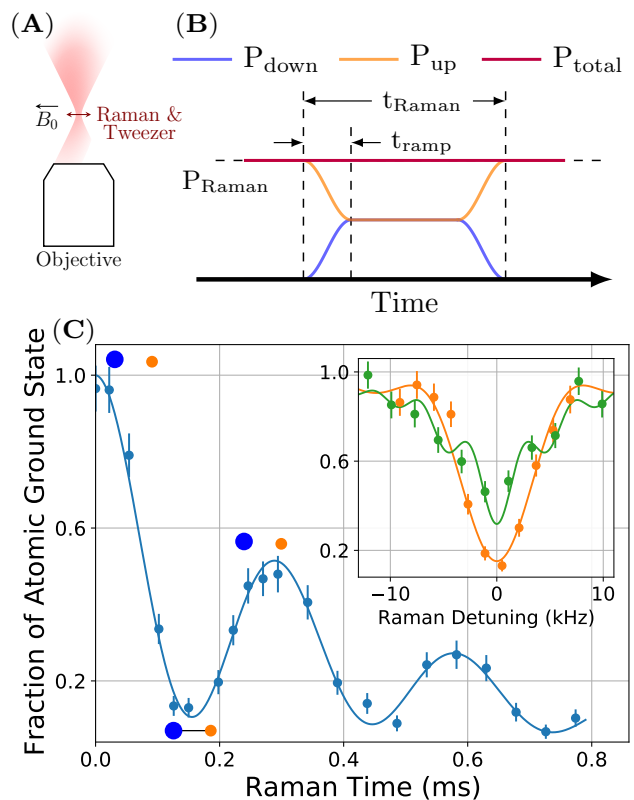


FIG. 2. (A) Geometry and polarization of trap and Raman beam relative to the bias magnetic field. The tweezer and Raman beam is focused through an objective to define the location of the atoms and molecule. We use a bias B field of $B_0 = 8.8G$ alone the tweezer polarization to define the quantization axis. As a result, the atoms experiences predominately $\pi$ polarization from the tweezer. (B) Molecule formation pulse sequence. The tweezer initially consists of only up leg power. When driving the Raman transition, the up leg power is smoothly ramped down and the down leg power ramped up over $10\mu s$ while maintaining the total power of the tweezer. This minimizes the heating on the atoms due to power fluctuation while maximizes the time with maximum Raman Rabi frequency when the up and down leg powers are equal. (C) Raman pulse time scan on resonance. A decaying Rabi oscillation can be observed proving the coherence of the Raman transfer process. Inset: Raman detuning scans at different times showing the resonance frequency. This is also fitted to a model of Raman transition with loss on the atom and molecule state and is used to determine both the Raman Rabi frequency and the loss rates.

remains unchanged. Both frequencies are kept on for a specified duration before the process is reversed and the tweezer returns to a single frequency. Furthermore, we use a Bragg grating with a linewidth (FWHM) of 50 GHz to filter the laser spectrum generated by a fiber amplifier that is seeded with a 1037 nm external cavity diode laser. We observed a reduction of the scattering rate by a factor of 2 due to suppression of the broadband amplified spontaneous emission (ASE) from the laser that couples
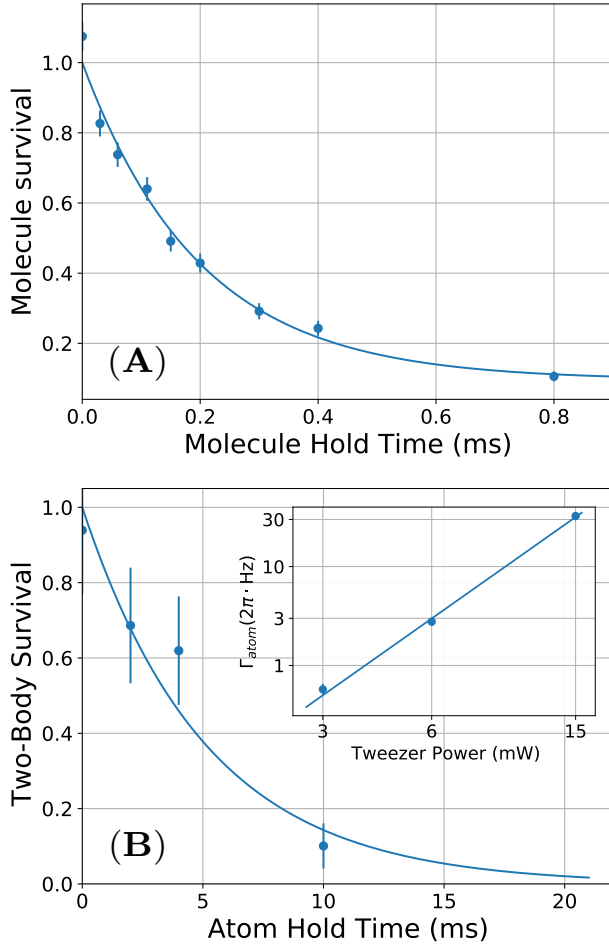
FIG. 3. (A) Direct measurement of molecule lifetime in 15mW of trap depth. Molecule survival is detected by dissociating back to atoms using a second Raman transition. The lifetime is consistent with the 0.1990(90)ms measured from the Raman transition data. The oscillation in the survival is the result of the interference between the two Raman pulses with incomplete transfer. (B) Two-body atom lifetime of 5.1(11)ms in 15mW of trap depth caused by off-resonance photoassociation. This is used to improve the fitting of the Raman transfer data. Inset: Atomic scattering rate scales as $P_{tweezer}^{2.58}$ on a log-log scale, this is consistent with a two photon scattering process. We have not measured a clear dependency of the loss rate on the tweezer detuning.

to other excited states.

We choose the tweezer frequency to be far detuned (145 GHz) from the $v' = 0$ line, and guided by coupled channel calculations, we locate the Raman resonance for the atom to molecule transition at 770.571504(85) MHz (Fig. 2C inset) with 15 mW tweezer power. The molecular state is dark to the imaging step, so successful transfer of the atoms to the molecular state will be detected as loss. We observed a Fourier limited linewidth which is evidence of a coherent transfer. In order to verify the coherence of the transfer directly, we fix the two

photon detuning on resonance and scan the pulse time. Fig. 2C shows the observed coherent Rabi oscillation between the atomic and molecular states. Fitting the data with a decaying Rabi oscillation suggests that 69% of initial ground state atoms are transferred into the molecular state. This transfer efficiency is mainly limited by the molecular lifetime which can be measured directly by preparing the molecule with a $\pi$ pulse and then using a second $\pi$ pulse to dissociate the molecule back to atoms after a variable wait time (Fig. 3A). The result shows a molecular lifetime of 0.1990(90)ms consistent with the decay of Rabi oscillation. We obtain the Raman Rabi frequency by fitting our measurements to a model that includes a Raman Rabi frequency and a finite lifetime for the molecular state (Fig. 2C and inset). We account for the effect of atomic state loss by measuring the one and two body lifetime of the atoms directly (Fig. 3B) without turning on the second frequency. The fit shows that we have a Raman Rabi frequency of $2\pi \times 3.282(42)$ kHz.

The efficiency of the transfer is worse than expected from theory and arises from the ratio of the molecule scattering rate to the Rabi frequency being 10 times larger than predicted. Based on the discussion above, if this discrepancy arises from the $v' = 0$ excited state, it can be either due to a high ratio of $\Omega_m/\Omega_a$ or a large $\Gamma_e$. Additionally, coupling to other excited states can also add an offset to both the Raman Rabi frequency and the scattering rate which can affect the scattering rate to Rabi frequency ratio.

In order to verify whether any one of these known sources are the origin of the discrepancy, we measured the Raman resonance as a function of the tweezer power and single photon frequency. These dependencies allow us to experimentally determine the matrix elements, $\Omega_a$, $\Omega_m$ and how much of the scattering, Stark shift, or Raman Rabi frequency comes from the $v' = 0$ intermediate state.

First we look at the change in resonance frequency. As a function of the tweezer power, we observe the expected linear dependency on the resonance frequency caused by the differential light shift between the atomic and molecular state (Fig. 4A). When we vary the tweezer frequency around the $v' = 0$ intermediate state, we can further observe a $1/\Delta$ component and a constant background in the experimentally explored region. The background is caused by coupling to other excited states that are further away in energy. The $1/\Delta$ component, however, is due to the coupling between the molecular state and the $v' = 0$ intermediate state. From this measurement, we can extract a $\Omega_m$ of $2\pi \times 36.162(20)$ MHz/$\sqrt{\text{mW}}$ or $2\pi \times 140.056(78)$ MHz for the 15 mW tweezer power used above. This number is consistent with the value of $2\pi \times 27\text{MHz}/\sqrt{\text{mW}}$ calculated from theory.

In order to calculate the matrix element ratio, we now need to extract the matrix element, $\Omega_a$. We do this by measuring the dependencies of the Raman Rabi fre-
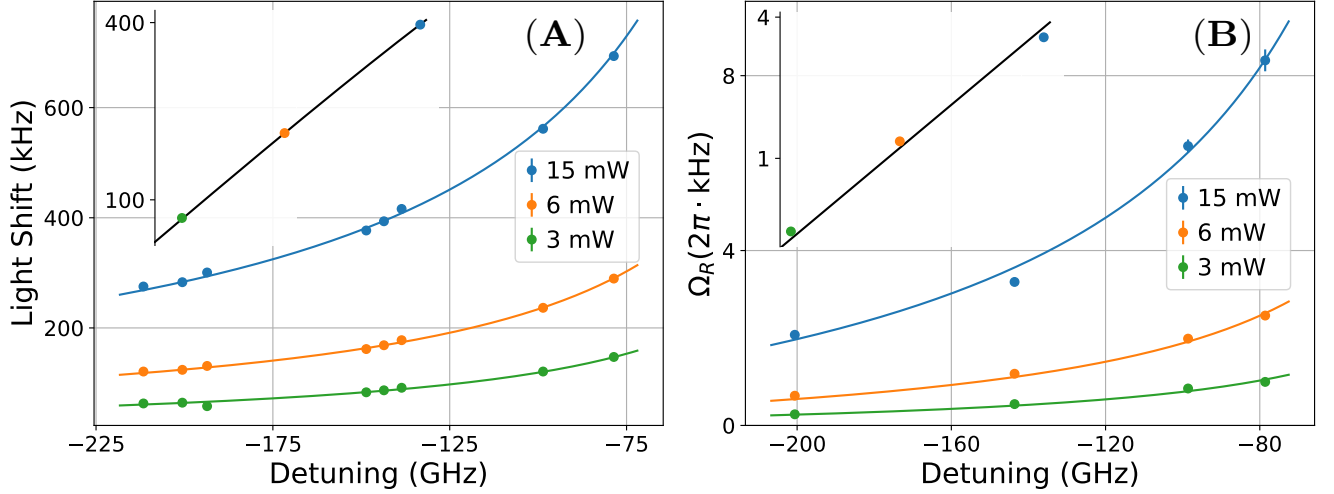
FIG. 4. Raman transition parameters as a function of tweezer and Raman power and detuning. The detuning is calculated from the closest $v' = 0$ PA frequency at 288703.6GHz. (A) The light shift of the Raman resonance scales as $P_{tweezer}$ and follows $1/\Delta$ with an offset. The fit also includes a small term that is proportional to $P_{tweezer}^2$ which is caused by the effective magnetic field generated by the tweezer which is perpendicular to the real magnetic field. (B) Raman Rabi frequency ($\Omega_R$) scales as $P_{tweezer}^{1.29}$ and follows $1/\Delta$ with an offset. From these results we can confirm the theory prediction of the atom-molecule matrix element ratio. Insets for (A) and (B), light shift and Raman Rabi frequency on a log-log plot showing the power law scaling.

quency, which depends on both $\Omega_m$ and $\Omega_a$. The Raman Rabi frequency shows a non-linear dependency on the tweezer power due to the change in the atomic wavefunction caused by tighter confinement at higher power (Fig. 4B). Thus, as discussed before, for weakly interacting particles, $\Omega_a$ scales as $\omega_{\text{trap}}^{3/4}$ or $P^{0.375}$. However, due to the strong interaction between the two atoms, this approximation breaks down. Instead, coupled-channel calculation shows that the scaling is very well approximated by $P^{0.29}$ within the range of confinement in our experiment. Combined with the standard intensity factor, the Raman Rabi frequency should scale as $P^{1.29}$, which agrees with our experimental result. Similar to the light shift, there is also a constant background component and a $v' = 0$ component in the Raman Rabi frequency that scales as $1/\Delta$. The $v' = 0$ component of the Raman Rabi frequency is $2\pi \times 170.0(39)$ Hz $\cdot$ mW$^{-1.29}$, or $2\pi \times 5.59(13)$ kHz at 15 mW tweezer power. Together with the $\Omega_m$ measured above, the up leg Rabi frequency is $2\pi \times 12.11(28)$MHz. This gives a Rabi frequency, and therefore matrix element, ratio of 11.59(26), which is in fact better than the theory prediction of 23.7 and should not cause the ratio of the Raman Rabi frequency to scattering rate from the $v' = 0$ state to be higher than expected. Furthermore, we measure the natural linewidth of the $v' = 0$ excited state to be no larger than 20MHz using photoassociation (PA) spectroscopy. This suggests that the excited state linewidth should not cause a stronger than expected scattering from $v' = 0$ state either.

With the $v' = 0$ state ruled out as the source of discrep-

ancy between experiment and theory, we now consider the background effects from other states with larger single photon detuning. Unfortunately, the background in the Raman Rabi frequency fit cancels the Rabi frequency for a single photon detuning that is red of the $v' = 0$ and reduces it by about 30% at the current detuning. However, this difference is not enough to explain the over factor of 10 discrepancy present in the experiment. The same offset will increase the Rabi frequency for blue detuning, but we have observed additional excited states at slightly higher frequencies which prevent the blue side of the transition to be usable for the Raman transition.

These results suggest that the decoherence or loss we observed during the Raman transition comes from either a higher than expected background scattering rate or a different intrinsic or technical source that we have not accounted for. We have observed a significant decrease in the coherence time without the ASE filter, suggesting the spectral purity of the laser is a significant source of scattering. Another source of decoherence could result from fluctuations in the power ratio between the two beams resulting in a fluctuation in the resonance position. In the experiment, we only stabilize the total power of the tweezer.

In additional to calibrating the $\Omega_m$ and $\Omega_a$, the scattering rate of the molecule is also depend on the tweezer power and detuning. At 3mW tweezer power, we have observed molecule lifetime as long as 1ms. However, since the technical noise that can lead to decoherence is not fully characterized in our experiment, we are unable to further identify the source of the discrepancy based on

this dependency.

Lastly, to confirm that the excess scattering does not come from the atomic state, we measure the two-body scattering rate without turning on the second frequency (Fig. 3B inset). The scattering rate scales as $P_{tweezer}^{2.58}$ which is inconsistent with a single photon scattering process. We have not been able to observe a dependency on the detuning in order to verify if the scattering process is related to the $v' = 0$ state, but the power scaling strongly suggests the existence of a unknown two photon scattering process. Nevertheless, the absolute scattering rate is much lower than the total scattering rate and is not the limiting factor in our experiment.

B field dependency $42.17(24)kHz/G$.

In conclusion, we have formed a weakly bound NaCs molecule in an optical tweezer via an optical Raman transfer. A theoretical investigation including all excited states of $c^3\Sigma^+(\Omega = 1)$, the excited atomic continuum and coupled channel ground state wavefunctions indicated better transfer efficiency using a deeply bound intermediate state and the $|\uparrow_{Na}\downarrow_{Cs}\rangle$ hyperfine state combination. Using these theoretical insights, we located the weakly bound state and coherently associated the atoms into the weakly bound molecule. Our transfer efficiency is limited by an unknown scattering source resulting in measured scattering rates over 10 times larger than theory predictions. Despite this limitation, the transfer efficiency may be further improved by increasing the $\Omega_a/\Omega_m$ ratio by exploring the possibility of driving to more deeply bound states. There may also be a better choice of single photon detuning to increase the Raman Rabi frequency, since our location results in about 30% cancellation of the Raman Rabi frequency due to an offset of unknown origin. Nevertheless, our technique, with the right choice of parameters, can be used to form a more diverse set of molecular species, since it does not rely on a magnetic Feshbach resonance, bound states at the MHz-level or a narrow excited state. The formation of a weakly bound molecule is a key step in forming rovibrational ground state molecules. Combined with real time rearrangement [50, 51], defect free arrays of highly controlled molecules can be formed in arbitrary geometries. These arrays are a promising and flexible platform for quantum simulation and quantum computing applications.

* yichaoyu@g.harvard.edu
† ni@chemistry.harvard.edu

[1] S. S. Kondov, C.-H. Lee, K. H. Leung, C. Liedl, I. Majewska, R. Moszynski, and T. Zelevinsky, Nature Physics 15, 1118–1122 (2019).
[2] I. Kozyryev and N. R. Hutzler, Physical Review Letters 119, 133002 (2017), publisher: American Physical Society.
[3] V. V. Flambaum and V. A. Dzuba, Phys. Rev. A 101, 042504 (2020).
[4] V. Andreev, D. G. Ang, D. DeMille, J. M. Doyle, G. Gabrielse, J. Haefner, N. R. Hutzler, Z. Lasner, C. Meisenhelder, B. R. O'Leary, C. D. Panda, A. D. West, E. P. West, X. Wu, and A. C. M. E. Collaboration, Nature 562, 355 (2018).
[5] W. B. Cairncross, D. N. Gresh, M. Grau, K. C. Cossel, T. S. Roussy, Y. Ni, Y. Zhou, J. Ye, and E. A. Cornell, Phys. Rev. Lett. 119, 153001 (2017).
[6] J. J. Hudson, D. M. Kara, I. J. Smallman, B. E. Sauer, M. R. Tarbutt, and E. A. Hinds, Nature 473, 493 (2011).
[7] N. Y. Yao, M. P. Zaletel, D. M. Stamper-Kurn, and A. Vishwanath, Nature Physics 14, 405 (2018).
[8] M. L. Wall, K. R. A. Hazzard, and A. M. Rey, From atomic to mesoscale: The role of quantum coherence in systems of various complexities (World Scientific, 2015) Chap. Quantum magnetism with ultracold molecules.
[9] B. Sundar, B. Gadway, and K. R. A. Hazzard, Scientific Reports 8, 3422 (2018).
[10] M. Wall, K. Maeda, and L. D. Carr, New Journal of Physics 17, 025001 (2015).
[11] D. DeMille, Phys. Rev. Lett. 88, 067901 (2002).
[12] K.-K. Ni, T. Rosenband, and D. D. Grimes, Chem. Sci. 9, 6830 (2018).
[13] E. R. Hudson and W. C. Campbell, Phys. Rev. A 98, 040302(R) (2018).
[14] Y. Lin, D. R. Leibrandt, D. Leibfried, and C.-W. Chou, Nature 581, 273 (2020).
[15] J. L. Bohn, A. M. Rey, and J. Ye, Science 357, 1002 (2017).
[16] N. Balakrishnan, J. Chem. Phys. 145, 150901 (2016), http://dx.doi.org/10.1063/1.4964096.
[17] M.-G. Hu, Y. Liu, D. D. Grimes, Y.-W. Lin, A. H. Gheorghe, R. Vexiau, N. Bouloufa-Maafa, O. Dulieu, T. Rosenband, and K.-K. Ni, Science 366, 1111 (2019), https://science.sciencemag.org/content/366/6469/1111.full.pdf.
[18] Y. Segev, M. Pitzer, M. Karpov, N. Akerman, J. Narevicius, and E. Narevicius, Nature 572, 189 (2019).
[19] E. B. Norrgard, D. J. McCarron, M. H. Steinecker, M. R. Tarbutt, and D. DeMille, Phys. Rev. Lett. 116, 063004 (2016).
[20] L. Anderegg, B. L. Augenbraun, Y. Bao, S. Burchesky, L. W. Cheuk, W. Ketterle, and J. M. Doyle, Nature Physics 14, 890 (2018).
[21] D. Mitra, N. B. Vilas, C. Hallas, L. Anderegg, B. L. Augenbraun, L. Baum, C. Miller, S. Raval, and J. M. Doyle, Science 369, 1366 (2020), https://science.sciencemag.org/content/369/6509/1366.full.pdf.
[22] S. Ding, Y. Wu, I. A. Finneran, J. J. Burau, and J. Ye,

Phys. Rev. X **10**, 021049 (2020).

[23] D. J. McCarron, M. H. Steinecker, Y. Zhu, and D. De-Mille, Phys. Rev. Lett. **121**, 013202 (2018).

[24] J. Lim, J. R. Almond, M. A. Trigatzis, J. A. Devlin, N. J. Fitch, B. E. Sauer, M. R. Tarbutt, and E. A. Hinds, Phys. Rev. Lett. **120**, 123201 (2018).

[25] L. De Marco, G. Valtolina, K. Matsuda, W. G. Tobias, J. P. Covey, and J. Ye, Science **363**, 853 (2019), https://science.sciencemag.org/content/363/6429/853.full.pdf.

[26] J. T. Zhang, Y. Yu, W. B. Cairncross, K. Wang, L. R. B. Picard, J. D. Hood, Y.-W. Lin, J. M. Hutson, and K.-K. Ni, Phys. Rev. Lett. **124**, 253401 (2020).

[27] X. He, K. Wang, J. Zhuang, P. Xu, X. Gao, R. Guo, C. Sheng, M. Liu, J. Wang, J. Li, G. V. Shlyapnikov, and M. Zhan, Science **370**, 331 (2020), https://science.sciencemag.org/content/370/6514/331.full.pdf.

[28] J. G. Danzl, E. Haller, M. Gustavsson, M. J. Mark, R. Hart, N. Bouloufa, O. Dulieu, H. Ritsch, and H.-C. Nägerl, Science **321**, 1062 (2008).

[29] K.-K. Ni, S. Ospelkaus, M. H. G. de Miranda, A. Pe'er, B. Neyenhuis, J. J. Zirbel, S. Kotochigova, P. S. Julienne, D. S. Jin, and J. Ye, Science **322**, 231 (2008).

[30] F. Lang, K. Winkler, C. Strauss, R. Grimm, and J. Hecker Denschlag, Phys. Rev. Lett. **101**, 133005 (2008).

[31] T. Takekoshi, L. Reichsöllner, A. Schindewolf, J. M. Hutson, C. R. Le Sueur, O. Dulieu, F. Ferlaino, R. Grimm, and H.-C. Nägerl, Phys. Rev. Lett. **113**, 205301 (2014).

[32] P. K. Molony, P. D. Gregory, Z. Ji, B. Lu, M. P. Köppinger, C. R. Le Sueur, C. L. Blackley, J. M. Hutson, and S. L. Cornish, Phys. Rev. Lett. **113**, 255301 (2014).

[33] J. W. Park, S. A. Will, and M. W. Zwierlein, Phys. Rev. Lett. **114**, 205302 (2015).

[34] M. Guo, B. Zhu, B. Lu, X. Ye, F. Wang, R. Vexiau, N. Bouloufa-Maafa, G. Quéméner, O. Dulieu, and D. Wang, Phys. Rev. Lett. **116**, 205303 (2016).

[35] K. K. Voges, P. Gersema, M. Meyer zum Alten Borgloh, T. A. Schulze, T. Hartmann, A. Zenesini, and S. Ospelkaus, Phys. Rev. Lett. **125**, 083401 (2020).

[36] G. Reinaudi, C. B. Osborn, M. McDonald, S. Kotochigova, and T. Zelevinsky, Phys. Rev. Lett. **109**, 115303 (2012).

[37] S. Stellmer, B. Pasquiou, R. Grimm, and F. Schreck, Phys. Rev. Lett. **109**, 115302 (2012).

[38] D. J. Wineland, M. Barrett, J. Britton, J. Chi-

averini, B. DeMarco, W. M. Itano, B. Jelenković, C. Langer, D. Leibfried, V. Meyer, T. Rosenband, and T. Schätz, Philosophical Transactions of the Royal Society of London A: Mathematical, Physical and Engineering Sciences **361**, 1349 (2003), http://rsta.royalsocietypublishing.org/content/361/1808/1349.full.pdf.

[39] We choose the two beams to have equal power, which gives the highest Raman Rabi rate at a fixed total power. Thus, this results in a simple factor of 2 coming from scattering off 2 beams.

[40] R. Wynar, R. S. Freeland, D. J. Han, C. Ryu, and D. J. Heinzen, Science **287**, 1016 (2000), http://science.sciencemag.org/content/287/5455/1016.full.pdf.

[41] T. Rom, T. Best, O. Mandel, A. Widera, M. Greiner, T. W. Hänsch, and I. Bloch, Phys. Rev. Lett. **93**, 073002 (2004).

[42] A. Grochola, P. Kowalczyk, J. Szczepkowski, W. Jastrzebski, A. Wakim, P. Zabawa, and N. P. Bigelow, Phys. Rev. A **84**, 012507 (2011).

[43] L. R. Liu, J. T. Zhang, Y. Yu, N. R. Hutzler, Y. Liu, T. Rosenband, and K.-K. Ni, arXiv:1701.03121 .

[44] There is an additional factor of 2, with both beams at equal power, to account for the Stark shift caused by both beams.

[45] J. D. Hood, Y. Yu, Y.-W. Lin, J. T. Zhang, K. Wang, L. R. Liu, B. Gao, and K.-K. Ni, Phys. Rev. Research **2**, 023108 (2020).

[46] L. R. Liu, J. D. Hood, Y. Yu, J. T. Zhang, N. R. Hutzler, T. Rosenband, and K.-K. Ni, Science **360**, 900 (2018).

[47] L. R. Liu, J. D. Hood, Y. Yu, J. T. Zhang, K. Wang, Y.-W. Lin, T. Rosenband, and K.-K. Ni, Phys. Rev. X **9**, 021039 (2019).

[48] K. Wang, X. He, R. Guo, P. Xu, C. Sheng, J. Zhuang, Z. Xiong, M. Liu, J. Wang, and M. Zhan, Phys. Rev. A **100**, 063429 (2019).

[49] This interaction shift is larger than the differential axial trapping frequency between Na and Cs atoms, which decouples the relative and center of mass motional state and improves the robustness of our preparation of the relative motion ground state.

[50] D. Barredo, S. de Léséleuc, V. Lienhard, T. Lahaye, and A. Browaeys, Science **354**, 1021 (2016).

[51] M. Endres, H. Bernien, A. Keesling, H. Levine, E. R. Anschuetz, A. Krajenbrink, C. Senko, V. Vuletic, M. Greiner, and M. D. Lukin, Science **354**, 1024 (2016).